Available online at www.sciencedirect.com
SCIENCE DIRECT
ELSEVIER
Coordination Chemistry Reviews 250 (2006) 1642–1652
COORDINATION CHEMISTRY REVIEWS
www.elsevier.com/locate/ccr

Review

Low-temperature lifetimes of metastable high-spin states in spin-crossover and in low-spin iron(II) compounds: The rule and exceptions to the rule

Andreas Hauser [a,*], Cristian Enachescu [b], Max Lawson Daku [a], Alfredo Vargas [a], Nahid Amstutz [a]

[a] *Département de Chimie Physique, Université de Genève, 30 quai Ernest-Ansermet, 1211 Genève 4, Switzerland*
[b] *Department of Solid State and Theoretical Physics, "Alexandru Ioan Cuza" University 11 Blvd. Carol, R-700506 Iasi, Romania*

Received 6 September 2005; accepted 11 December 2005
Available online 18 January 2006

Contents

Abstract

The high-spin → low-spin relaxation in spin-crossover compounds can be described as non-adiabatic multi-phonon process in the strong coupling limit, in which the low-temperature tunnelling rate increases exponentially with the zero-point energy difference between the two states. Based on the hypothesis that the experimental bond length difference between the high-spin and the low-spin state of ~0.2 Å is also valid for low-spin iron(II) complexes, extrapolation of the single configurational coordinate model allows an estimate of the zero-point energy difference for low-spin complexes from kinetic data. DFT calculations on low-spin $[Fe(bpy)_3]^{2+}$ support the structural assumption. However, for low-spin $[Fe(terpy)_2]^{2+}$ the relaxation rate constant shows an anomalous behaviour in so far as it is more in line with spin-crossover systems. This is attributed to very anisotropic bond length changes associated with the spin state change, and the subsequent breakdown of the single mode model.

Keywords: Spin-crossover; Intersystem crossing; Radiationless relaxation; Density functional theory; Iron(II)-tris-2,2′-bipyridine; Iron(II)-bis-2,2′:6′,2″-terpyridine

1. Introduction

Over the past decades, complexes of transition metal ions having a d^4–d^7 electronic configuration and showing the phenomenon of thermal spin-crossover have received increasing attention because of their potential applications as molecular switches in information storage and display devices [1]. Such complexes are characterised by two low-lying electronic states of different spin-multiplicities: the low-spin (LS) state with a maximum number of paired up electrons in the t_{2g} subshell as the electronic ground state, and the high-spin (HS) state with the electrons entering the d-orbitals according to Hund's rule as thermally accessible state at comparatively low temperatures. For octahedral iron(II) complexes, these states are the low-spin $^1A_1(t_{2g}^6)$ state and the high-spin $^5T_2(t_{2g}^4e_g^2)$ state. The thermal spin transition is entropy driven and occurs from the low-spin state populated at low temperatures to an almost quantitative population of the high-spin state at elevated temperatures. The temperature at which the fraction of complexes in the high-spin state $\gamma_{HS} = 1/2$, generally referred to the transition tempera-

* Corresponding author. Tel.: +41 22 379 6559; fax: +41 22 379 6103.
E-mail address: andreas.hauser@unige.ch (A. Hauser).

0010-8545/$ – see front matter © 2005 Elsevier B.V. All rights reserved.
doi:10.1016/j.ccr.2005.12.006

ture $T_{1/2}$, is a measure for the difference in zero-point energy $\Delta E^0_{HL} = E^0_{HS} - E^0_{LS}$ between the two states. In dilute systems, that is in liquid or rigid solutions as well as in doped crystalline materials, the thermal spin transition is gradual corresponding to a Boltzmann distribution between the two vibronic manifolds. In neat spin-crossover compounds, transition curves tend to be more abrupt and may occur as first order phase transitions with a hysteresis. Such a cooperative behaviour is due to elastic interactions between the spin-crossover complexes which result from the comparatively large differences in molecular geometry between the two states. For iron(II) complexes it is essentially the metal–ligand bond lengths which are most affected by the spin transition, with typical values of the bond length difference $\Delta r_{HL} = r_{HS} - r_{LS} \approx 0.2$ Å [2], due to the transfer of two electrons to the anti-bonding e_g orbitals and concurrent loss of π back bonding from the t_{2g} orbitals.

In addition to the thermal spin transition, an efficient light-induced population of the high-spin state can be effected well below the thermal spin transition by irradiating either into the spin-allowed d–d bands or the intense metal–ligand charge transfer (MLCT) band of the low-spin species. As shown in Fig. 1, the initially excited state is extremely short-lived and decays within less than a picosecond [3] and with a quantum efficiency close to unity non-radiatively to the high-spin state. This effect has been extensively used to monitor the intersystem crossing dynamics of spin-crossover complexes not only in solution at around ambient temperature where for iron(II) they occur on the microsecond time scale [4,5], but also in the solid state. In the solid state at sufficiently low temperatures, the energy barrier effectively traps the complexes in the high-spin state, often with lifetimes of several days, an effect now currently referred to as "light-induced excited spin-state trapping" and known under the acronym of LIESST [6,7]. The light-induced high-spin state shows the same increase of ~0.2 Å in metal–ligand bond length as the thermally populated high-spin state [8].

In 1980, Buhks et al. [9], laid the theoretical foundations for the description of the high-spin → low-spin intersystem crossing process in spin-crossover complexes as a non-adiabatic multiphonon process in the strong coupling region, characterised by a large geometrical rearrangement along the relevant reaction coordinate together with a small driving force. Buhks et al. predicted a temperature independent tunnelling process at low temperatures and a thermally activated process at elevated temperatures. In 1987, Xie and Hendrickson [10] presented the first experimental evidence for the low-temperature tunnelling process. This was followed by a series of papers by Hauser et al. [11], which systematically explored the geometric and energetic parameters governing the low-temperature tunnelling rate constant and how this rate constant can be tuned both chemically and physically chiefly in iron(II) spin-crossover and low-spin systems. Chemically, of course, this can be achieved by substitutions on the ligand sphere. Due to the above mentioned large difference in metal–ligand bond length and the concomitant large difference in molecular volume $\Delta V_{HL} = V_{HS} - V_{LS} \approx 25$ Å^3 per complex [12], external pressure as well as lattice effects may likewise be used to tune both the transition temperature as well as the high-spin → low-spin relaxation rate constant.

In the present paper we begin with a brief summary of the theory of Buhks et al. and its application to iron(II) spin-crossover systems. We show how the extrapolation to low-spin systems helps locate the energy of the spectroscopically inaccessible high-spin state of the low-spin $[Fe(bpy)_3]^{2+}$ complex (bpy = 2,2′-bipyridine), and we discuss the reason for the apparent breakdown of the theory for the low-spin complex $[Fe(terpy)_2]^{2+}$ (terpy = 2,2′:6′,2″-terpyridine). DFT calculations of the geometry and the energetics of the two states for both complexes will serve to underline the conclusions.

2. Results and discussion

2.1. The rule

Fig. 1 shows the potential wells of the high-spin and the low-spin states of typical iron(II) spin-crossover as well as low-spin

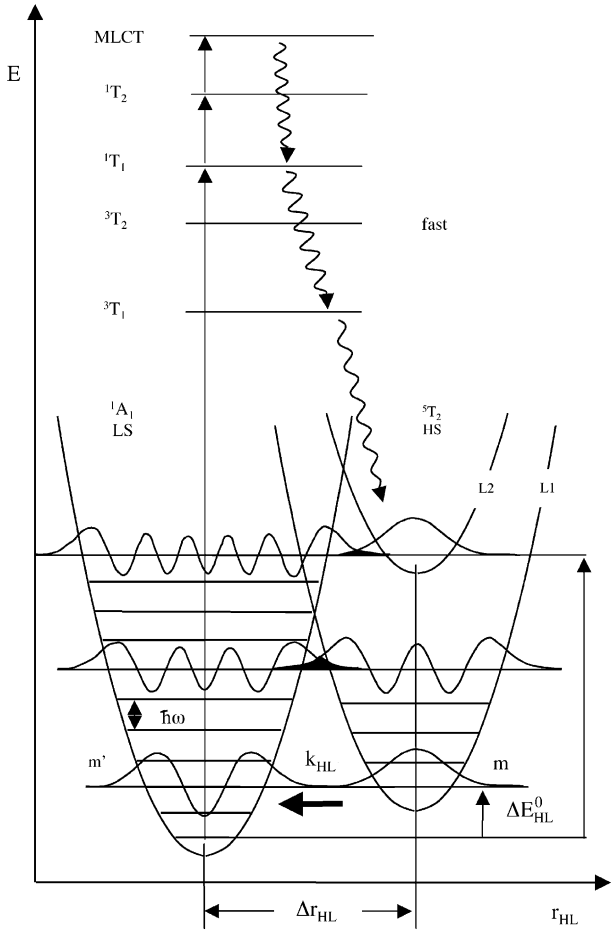

Fig. 1. The electronic structure of iron(II) spin-crossover (ligand L1) and low-spin complexes (ligand L2). The mechanisms for the light-induced population of the high-spin state following excitation into ligand-field or MLCT bands of the low-spin species are indicated by curly arrows. At low temperatures the barrier effectively traps the complex in the high-spin state. Potential wells of the high-spin and the low-spin state are shown along the totally symmetric normal coordinate. At low temperatures tunnelling occurs exclusively from the lowest vibrational state of the high-spin state. At elevated temperatures, tunnelling occurs as an activated process from thermally populated vibrational levels of the high-spin state. The zero-point energy difference ΔE^0_{HL} can be tuned chemically and physically.

compounds. The reaction coordinate Q for the spin transition is best described by a single normal mode, that is, the totally symmetric breathing mode. In terms of metal–ligand bond length difference, the horizontal displacement of the two potential wells relative to each other $\Delta Q_{HL} = \sqrt{6}\,\Delta r_{HL} \approx 0.5$ Å . Classically, complexes trapped in the high-spin state would have to acquire enough thermal energy to pass over the top of the energy barrier. Quantum mechanically, the rate constant for a tunnelling process is given by [13]

$$k_{HL}(T) = \frac{2\pi}{\hbar^2\omega}\beta_{HL}^2 F_n(T) \quad (1)$$

where the thermally averaged Franck–Condon factor is given by

$$F_n(T) = \frac{\sum_m |\langle\chi_{m+n}|\chi_m\rangle|^2\, e^{-m\hbar\omega/k_B T}}{\sum_m e^{-m\hbar\omega/k_B T}} \quad (2)$$

The electronic coupling matrix element $\beta_{HL} = \langle\Phi_{LS}|H_{SO}|\Phi_{HS}\rangle \sim 150\,cm^{-1}$ is given by second order spin–orbit coupling [9], $\hbar\omega$ of typically of $\sim$250 cm^{-1} is the vibrational frequency of the active vibration, $|\langle\chi_{m'}|\chi_m\rangle|^2$ is the Franck–Condon factor of the overlap of the vibrational wavefunctions of the low-spin and the high-spin state at the corresponding energy. If, for mathematical simplicity, harmonic potentials with equal force constants and vibrational frequencies are assumed for the two states, energy conservation requires that $m' = m + n$, where $n = \Delta E_{HL}^0/\hbar\omega$ corresponds to the zero-point energy difference expressed in units of vibrational quanta. This quantity, commonly referred to as the reduced energy gap, is a dimensionless measure of the vertical displacement of the potential wells relative to each other.

At low temperatures, where only the vibrational ground state of the high-spin state is populated, the relaxation rate constant is given by

$$k_{HL}(T \to 0) = \frac{2\pi}{\hbar^2\omega}\beta_{HL}^2 |\langle\chi_n|\chi_0\rangle|^2 \quad (3)$$

In the case of the harmonic approximation with equal force constants the Franck–Condon factor from the lowest vibrational level of the high-spin state is given by [14]

$$|\langle\chi_n|\chi_0\rangle|^2 = \frac{S^n e^{-S}}{n!} \quad (4)$$

where

$$S = \frac{\frac{1}{2} f\,\Delta Q_{HL}^2}{\hbar\omega} \quad (5)$$

The quantity S, the so-called Huang–Rhys factor [14], is a dimensionless measure of the horizontal displacement of the potential wells relative to each other. For an average force constant of the order of 2×10^5 dyn/cm for the active vibration and using the above model parameters for the other quantities, the Huang–Rhys factor S takes on a value of $\sim$45. Both, β_{HL} and S are not expected to vary to a great extent within the class of iron(II) compounds having [FeN_6] coordination. ΔE_{HL}^0 and therefore n, however, vary quite substantially from compound to compound, as borne out by the range of values of spin transition temperature $T_{1/2}$. For low-spin compounds, ΔE_{HL}^0 is simply too large for a thermal population of the high-spin state at temperatures below the thermal decomposition, which for organometallic compounds rarely exceeds 600 K.

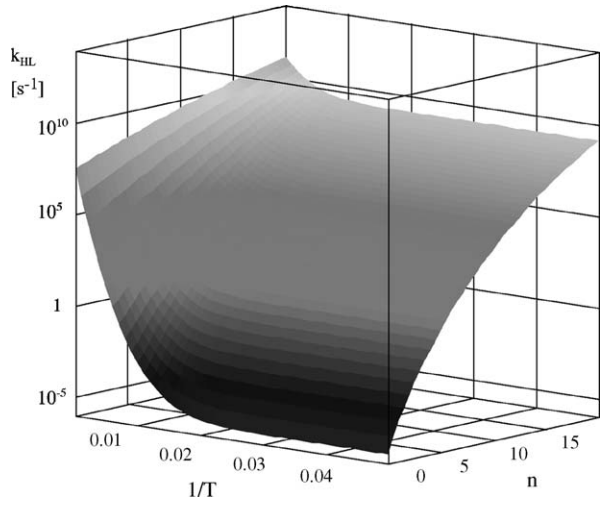

Fig. 2. The calculated relaxation rate constant k_{HL} plotted on a logarithmic scale as a function of $1/T$ and the reduced energy gap n according to Eq. (1). Model parameters: the Huang–Rhys factor $S = 45$, the vibrational frequency of the active vibration $\hbar\omega_1 \approx 250\,cm^{-1}$, and the electronic matrix element $\beta_{HL} = 150\,cm^{-1}$.

Fig. 2 shows the high-spin → low-spin relaxation rate constant, k_{HL}, on a logarithmic scale versus $1/T$ (Arrhenius plot) calculated according to Eq. (3) using the above standard set of values for S, β_{HL} and $\hbar\omega$, and with the reduced energy gap n as variable parameter. Below $\sim$50 K, the theory predicts a temperature independent process corresponding to pure tunnelling in which the electronic energy of the high-spin state is spontaneously transformed into vibrational energy in the low-spin state, followed by rapid and irreversible dispersion of this energy into the surrounding medium. For small values of n, the low-temperature tunnelling rate constant increases exponentially with n. At somewhat larger values of n, the increase becomes less dramatic, following the bell shaped curve of Marcus theory with, in principle, a maximum value as n approaches S [15].

2.2. The low-temperature tunnelling rate constant and extrapolation to low-spin complexes

As mentioned above, for spin-crossover compounds the thermal transition temperature $T_{1/2}$ is a measure for the zero-point energy difference ΔE_{HL}^0. The latter can approximately be set equal to the standard enthalpy difference between the two states, which, in turn, is related to the standard entropy difference and $T_{1/2}$ according to

$$\Delta E_{HL}^0 \approx \Delta H_{HL}^0 = \Delta S_{HL}^0 T_{1/2} \quad (6)$$

Even though ΔS_{HL}^0 varies from compound to compound, it does so in comparatively small range around 5 $cm^{-1}\,K^{-1}$. Fig. 3 shows the experimentally determined low-temperature tunnelling rate constant $k_{HL}(T \to 0)$ for a number of spin-crossover complexes taken from reference [11] plotted on a logarithmic scale versus ΔE_{HL}^0 as determined from the experimental values of $T_{1/2}$ according to Eq. (6) and using the

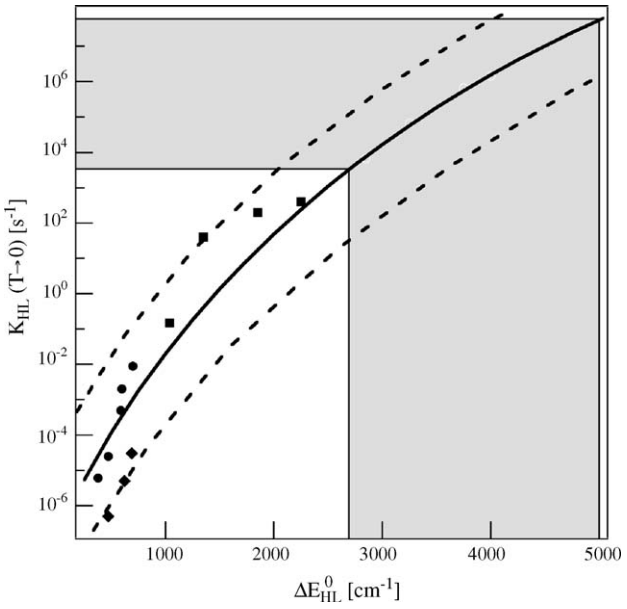

Fig. 3. Experimentally determined low-temperature tunnelling rate constants, $k_{HL}(T \rightarrow 0)$, for a number of spin-crossover complexes plotted on a logarithmic scale vs. ΔE^0_{HL} as determined from the experimental values of $T_{1/2}$ according to Eq. (6) and setting ΔS^0_{HL} to 5 cm^{-1} K^{-1} (●,♦, ■). All experimental values refer to diluted systems (doped crystalline solids, rigid solutions and diluted in polymer matrices) and are taken from Ref. [11]. Calculated curves using Eq. (3) and the model values as described in the text with an average value of $S = 45$ (—) and the limiting values 40 and 50 (– – –). The range of experimental values for the low-spin complex $[Fe(bpy)_3]^{2+}$ doped into different crystalline host lattices [16] is indicated by the shaded area.

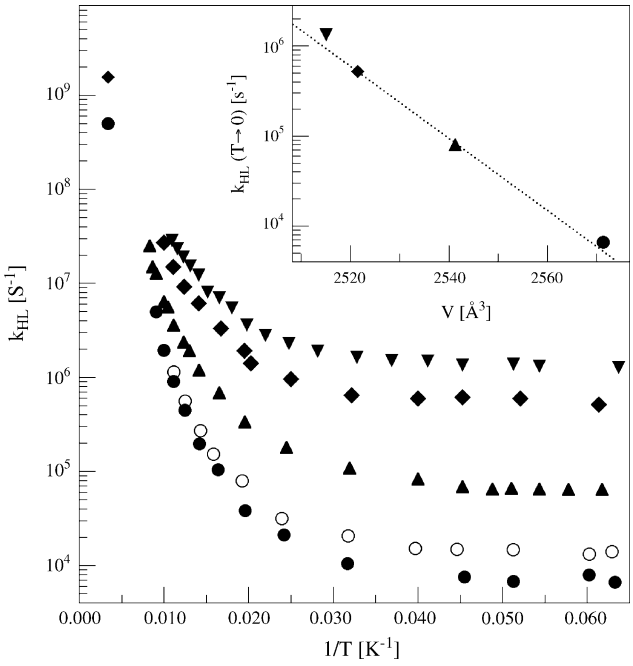

Fig. 4. The high-spin → low-spin relaxation rate constant kHL plotted on a logarithmic scale against $1/T$ (Arrhenius plot) for $[Fe(bpy)3]^{2+}$ doped into [M(bpy)3](PF6)2, M = Co (▼), Zn (♦), Mn (▲), and Cd (●) at ambient pressure, and for Cd at 1 kbar external pressure (◯). Insert: the low-temperature tunnelling rate constant $k_{HL}(T \rightarrow 0)$ vs. the unit cell volume of the host lattice for $[Fe(bpy)_3]^{2+}$ doped into [M(bpy)3](PF6)2, M = Co, Zn, Mn, Cd (adapted from Ref. [16]).

above model value for ΔS^0_{HL}. The range of observed rate constants $k_{HL}(T \rightarrow 0)$ goes from $<10^{-5}$ s^{-1} ($\tau > 1$ day) for $\Delta E^0_{HL} < 500$ cm^{-1} ($T_{1/2} < 100$ K) to $>10^3$ s^{-1} ($\tau < 1$ ms) for $\Delta E^0_{HL} > 2500$ cm^{-1} ($T_{1/2} > 500$ K). Fig. 3 includes $k_{HL}(T \rightarrow 0)$ calculated according to Eq. (3) using the above model values for the various parameters, in particular $S = 45$. The experimental values all fall within the narrow band calculated around $S = 45 \pm 5$.

The light-induced population of the high-spin state is also possible for low-spin compounds. For example, Kirk et al. [17] observed a transient state in the $[Fe(bpy)_3]^{2+}$ (bpy = 2,2′-trisbipyridine) complex at room temperature in aqueous solution with a lifetime of 0.83 ns. Although at the time Kirk et al. proposed a different state as metastable state, the comparison of Mössbauer emission data from $[^{57}Co(bpy)_3]^{2+}$ with data from pulsed laser excitation on $[Fe(bpy)_3]^{2+}$ both doped into $[Mn(bpy)_3](PF_6)_2$ unambiguously proved the light-induced metastable state to be the high-spin $^5T_2(t_{2g}{}^4e_g{}^2)$ state [18]. Fig. 4 shows the high-spin → low-spin relaxation rate constant, k_{HL}, on a logarithmic scale as a function of $1/T$ for $[Fe(bpy)_3]^{2+}$ doped into the series of isostructural hosts $[M(bpy)_3](PF_6)_2$, M = Co, Zn, Mn, and Cd at ambient pressure and for M = Cd additionally at an external pressure of 1 kbar. As predicted by Fig. 2, the larger driving force results in substantially larger low-temperature tunnelling rate constants than for the spin-crossover systems, and the activation energy is smaller. At room temperature, the value of k_{HL} for the doped systems is close to the value observed in solution and does not depend very much on the host. However, at low temperatures the rate constant depends very much on the host, ranging from 6×10^3 s^{-1} ($\tau = 160$ μs) for M = Cd to 1.6×10^6 s^{-1} ($\tau = 650$ ns) for M = Co, that is, it increases by a factor of almost 300 with decreasing unit cell volume of the host. As schematically shown in Fig. 5, this range of values is due to different lattice pressures, the smaller unit cell volumes effectively destabilising the high-spin state of the iron(II) complex with its larger molecular volume as compared to the one of the low-spin state [16]. By comparison with the effect of an external pressure of 1 kbar on the relaxation rate constant for the Cd host, the difference in lattice pressure in the series of hosts corresponds to the effect of an external pressure of ∼8 kbar. The above range of relaxation rate constants translates into a range for the zero-point energy difference between the two states. Based on the structural assumption that the reaction coordinate is also essentially given by the breathing mode, and that the value of Δr_{HL} of ∼0.2 Å for spin-crossover complexes with $[FeN_6]$ coordination is also transferable to low-spin complexes with the same first coordination sphere, the extrapolation using Fig. 2 gives a value for ΔE^0_{HL} for $[Fe(bpy)_3]^{2+}$ in the range 2500–5000 cm^{-1} for the present series of host lattices.

The structural hypothesis is not easy to verify experimentally. Density functional theory (DFT) [19–21] provides a theoretical approach to the problem as it allows the direct characterisation of the lowest-lying state of each spin and spatial symmetry, and with regard to geometry optimisation DFT is known to perform very well even for open shell systems [22]. Taking advantage of

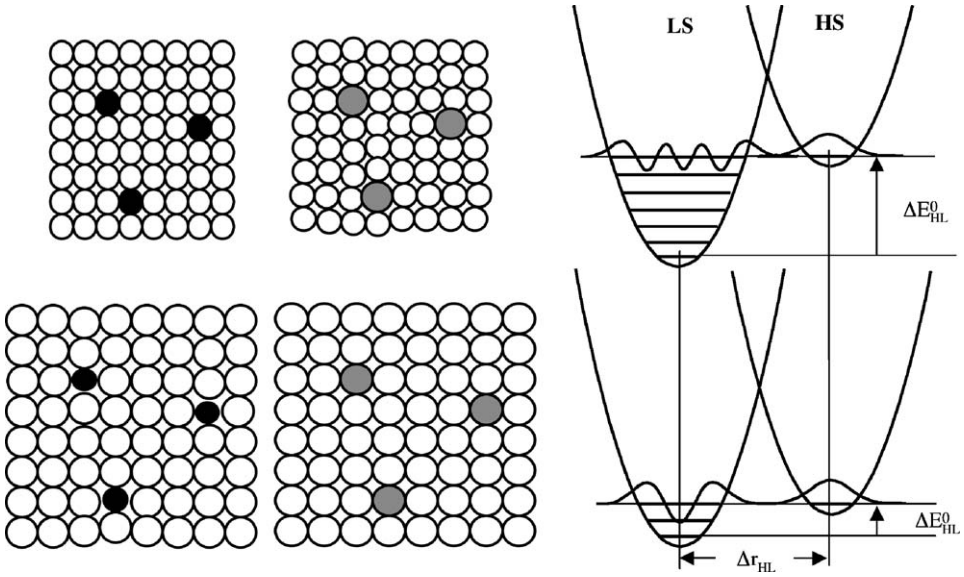

Fig. 5. Potential wells for an iron(II) complex doped into different host lattices, demonstrating the effect of different lattice pressures.

the fact that the low-spin and high-spin states of iron(II) complexes are the lowest-lying states of their respective spin multiplicities, the geometry of $[Fe(bpy)_3]^{2+}$ in the two spin-states was optimised using different exchange-correlation functionals as implemented in the Gaussian [23] and ADF [24,25] packages. In fact, all the different functionals give very similar results provided basis sets of high quality are used (see Ref. [26] for computational details). Table 1 gives average values as determined from the results obtained using the different functionals with basis sets of valence triple-ζ polarised quality, and Fig. 6 shows the overlaid structures of the two states. For the low-spin state the agreement of the calculated geometry with the experimental [27] geometry is remarkable. The only significant deviation concerns the rather floppy dihedral angle between the two rings of the bipyridine. As expected, the high-spin geometry is first of all characterised by a metal–nitrogen bond length which is much larger than for the low-spin state, that is $\Delta r_{HL} = 0.21$ Å. There is no indication of a spontaneous lowering of the symmetry in the high-spin state. Thus the basic structural assumption that the experimental value of Δr_{HL} of ~0.2 Å for spin-crossover compounds is transferable to low-spin compounds is validated by computational results from DFT. Of course, for the rather rigid bidentate bipyridine ligand the bite angle β and twist angle τ change quite considerably, too, in order to accommodate the large change in metal–nitrogen bond length.

Table 1
Selected experimental and calculated bond lengths (Å) and angles (°) of $[Fe(bpy)_3]^{2+}$ in the low-spin state, and calculated values for the complex in the high-spin state

	Experimental	Calculated	
		$^1A_{1g}(t_{2g}^6)$	$^5T_{2g}(t_{2g}^4e_g^2)$
Fe–N	1.967	1.981	2.192
N–C_2	1.359	1.367	1.380
N–C_6	1.338	1.354	1.368
C_2–C_2'	1.471	1.464	1.486
C_2–C_3	1.377	1.401	1.411
C_3–C_4	1.374	1.393	1.404
C_4–C_5	1.380	1.397	1.407
C_5–C_6	1.358	1.391	1.401
β	81.8	81.3	75.7
γ	6.4	1.5	4.3
τ	53.6	53.1	46.2
θ	57.8	58.0	59.1

The atom labelling and the definition of bond angles are shown in Fig. 6. Experimental values are taken from Ref. [27]. Calculated distances and angles are average values of the very similar DFT results obtained with different functionals and basis sets of valence triple-ζ polarised quality. For the high-spin state, average values of the two trigonal components are given. For details see Ref. [26].

The situation is not as clear-cut with regard to electronic energies of the two states relative to each other. In order to compare the calculated ΔE_{HL}^{el} values with the experimental estimate of ΔE_{HL}^{0}, the latter has to be corrected for the difference in zero-point vibrational energy between the two states, ΔE_{vib}^{0}, according to

$$\Delta E_{HL}^{0} = \Delta E_{HL}^{el} + \Delta E_{vib}^{0} \quad (7)$$

Due to a significant decrease in vibrational frequencies on going from the low-spin to the high-spin state, the vibrational contribution to the zero-point energy is substantially smaller for the high-spin state. ΔE_{vib}^{0} is typically on the order of $-1000\,cm^{-1}$. This gives an experimental estimate of ΔE_{HL}^{el} of 3500–6000 cm^{-1}. Table 2 gives the electronic energy difference between the high-spin and the low-spin state, $\Delta E_{HL}^{el} = E_{HS}^{el} - E_{LS}^{el}$, calculated for a number of different functionals using basis sets of valence triple-ζ polarised quality [26]. The calculated values depend very much on the functional used. In fact, most functionals fail to approach the experimental estimate. The large spread in calculated values of ΔE_{HL}^{el} was ascribed to the inability of the exchange part of the correlation-exchange functionals to properly account for the variation of exchange when the spin polarisation and the metal–ligand bond length significantly vary [26]. Thus, with the PBE, BP86, PW91 functionals which

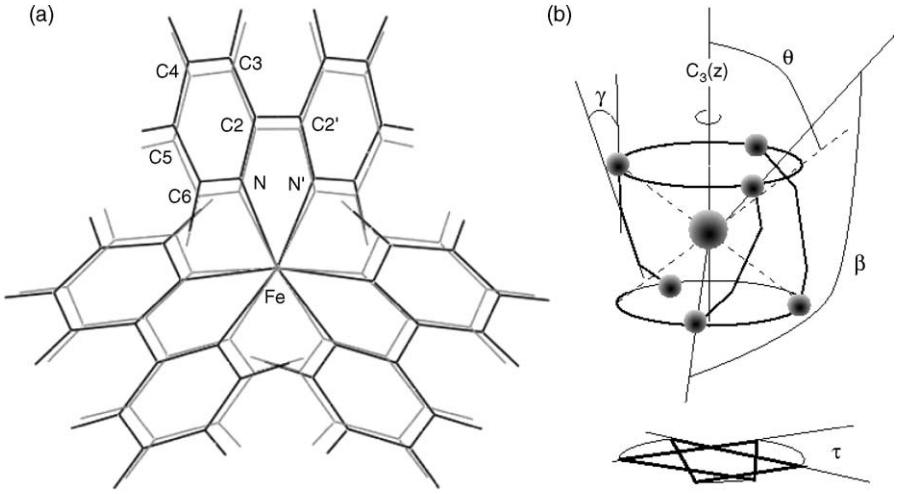

Fig. 6. (a) Overlaid calculated structures low-spin (grey) and high-spin (black) structures of $[Fe(bpy)_3]^{2+}$ projected along the molecular C_3 axis (RPBE,TZP) and (b) definition of angular parameters reported in Table 1.

are generalised gradient approximations (GGAs), the exchange is underestimated which translates into the overestimation of ΔE_{HL}^{el}. On the other hand, hybrid functionals, which incorporate Hartree–Fock exchange, tend to overestimate the exchange and thus to overstabilise the high-spin state. As a result they tend to underestimate ΔE_{HL}^{el}, some even predict $[Fe(bpy)_3]^{2+}$ to be a high-spin complex. The more recent RPBE GGA corrects for the underestimation of exchange, and gives the best results, along with the B3LYP* hybrid functional which conversely corrects for the overestimate of exchange of the other hybrids B3LYP and PBE0. Relative spin-state energetics thus provide a stringent criterion for assessing the performance of exchange-correlation functionals [26,28]. The results obtained for the spin-state energetics of $[Fe(bpy)_3]^{2+}$ are discussed in more detail in Ref. [26]. For our purpose, it suffices to retain that GGA and hybrid functionals give as expected an accurate and consistent description of both the low-spin and high-spin geometries of $[Fe(bpy)_3]^{2+}$, and that reliable results for the high-spin/low-spin energetics were obtained only with the RPBE and B3LYP* functionals, which give values for ΔE_{HL}^{el} of ~6800 and ~3400 cm^{-1}, respectively.

Table 2
The electronic energy difference (cm^{-1}) between the high-spin and low-spin states of $[Fe(bpy)_3]^{2+}$ calculated by DFT using Slater-type (TZP) and Gaussian-type (TZVP) basis sets of valence triple-ζ polarised quality and a number of different functionals available in ADF and Gaussian

	ΔE_{HL}^{el}	
	^5E	$^5A_1$
PBE/TZP	11022	11337
BP86/TZP	14397	15169
PW91/TZP	11699	11887
RPBE/TZP	6909	6640
PBE/TZVP		11373
B3LYP/TZVP		766
B3LYP*/TZVP		3432
PBE0/TZVP		−951

For details see Ref. [26].

2.3. A notable exception to the rule

Some 5 years ago, Renz et al. [29] realised that the low-spin $[Fe(terpy)_2]^{2+}$ (2,2′:6′,2″-terpyridine) complex shows LIESST like behaviour at low temperatures when doped into $[Mn(terpy)_2](ClO_4)_2$ with a low-temperature lifetime of the light-induced state of several hours instead of the expected microsecond range. As starting point for the badly needed explanation of this apparent breakdown of the theory, a systematic study of the high-spin → low-spin relaxation for this complex doped into various crystalline hosts, as pure compound dispersed in KBr and dissolved in the glass-forming mixture of acetonitrile/proprionitrile was undertaken. This is complemented with DFT calculations on the high-spin and the low-spin state of the complex.

Fig. 7 shows the single crystal absorption spectrum at 75 K of $[Zn(terpy)_2](PF_6)_2$ doped with $[Fe(terpy)_2]^{2+}$ at a level of 0.2 mol%. It is dominated by the intense MLCT absorption band of the iron(II) complex centred at 18 000 cm^{-1}. On lowering the temperature down to 10 K, the light of the lamp of the spectrom-

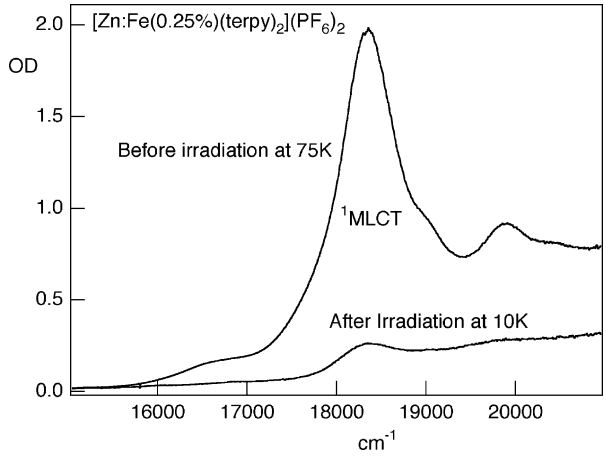

Fig. 7. Absorption spectra $[Zn:Fe(0.25\%)(terpy)_2](PF_6)_2$, at 50 K before and at 10 K after irradiation.

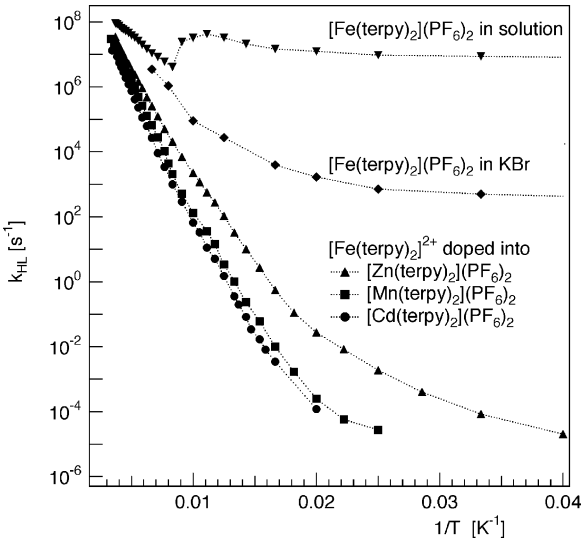

Fig. 8. High-spin → low-spin relaxation rate constants, k_{HL}, plotted on a logarithmic scale against $1/T$ for $[Fe(terpy)_2]^{2+}$ doped into $[M(terpy)_2](PF_6)_2$, M = Cd, Mn, and Zn, for $[Fe(terpy)_2](PF_6)_2$ dispersed in KBr, and dissolved in acetonitrile/proprionitrile mixture (glass point ∼150 K).

eter provides sufficient excitation to almost completely bleach the MLCT band within a few minutes, indicating a quantitative light-induced population of the high-spin state in this matrix. This is in contrast to the only partial light-induced population for the perchlorate host investigated by Renz et al. [29].

In the present system, the bleached spectrum persists for several hours, only when warming the sample to above 30 K does a noticeable relaxation set in, which can be monitored by optical spectroscopy. Corresponding relaxation curves are single exponential. Fig. 8 shows the high-spin → low-spin relaxation rate constants, k_{HL}, plotted on a logarithmic scale against $1/T$ not only for $[Fe(terpy)_2]^{2+}$ doped into $[Zn(terpy)_2](PF_6)_2$, but also into the isostructural $[Mn(terpy)_2](PF_6)_2$ and $[Cd(terpy)_2](PF_6)_2$ hosts as well as for $[Fe(terpy)_2](PF_6)_2$ dispersed into KBr, and in a acetonitrile/proprionitrile solution having a glass point of ∼150 K. At room temperature in solution, the lifetime is 23 ns ($k_{HL} = 4 \times 10^7\ s^{-1}$) [5] which is in accordance with the expectation for a low-spin complex, and likewise the apparent activation energy for the relaxation process is comparatively low. At the glass-point of the solvent mixture, the relaxation rate constant increases abruptly with decreasing temperature and reaches a low-temperature value of $10^7\ s^{-1}$ ($\tau = 100$ ns). This is a rather high value even for a low-spin complex. The behaviour dispersed in KBr corresponds closest to the expectation for a low-spin complex, with a value approaching the value measured in solution at room temperature, a still comparatively low activation energy and a plateau in the low-temperature tunnelling region with $k_{HL}(T \rightarrow 0) = 10^3\ s^{-1}$. For the three crystalline hosts $[M(terpy)_2](PF_6)_2$, M = Zn, Mn, Cd, the situation is quite different. At room temperature, the relaxation rate constants are not substantially smaller than in solution or for the neat compound, but the activation energy is much larger and the low-temperature tunnelling rate constants $k_{HL}(T \rightarrow 0) < 10^{-5}\ s^{-1}$, that is, in the range more typical for spin-crossover systems. As for $[Fe(bpy)_3]^{2+}$, the variation of the relaxation rate constant within the series of dilute mixed crystals can be attributed to the modulation of ΔE^0_{HL} by the lattice pressure. The same holds for the abrupt increase in rate constant upon formation of the much more rigid glass at the glass-point of the solvent mixture. But it is impossible to attribute the difference of more than 10 orders of magnitude in the relaxation rate constant between the doped crystalline materials and for $[Fe(terpy)_2]^{2+}$ in rigid solution to just a modulation of ΔE^0_{HL} by the different environments. Indeed, if such were the case, the doped crystalline materials would have to be in the range of spin-crossover systems, but temperature-dependent absorption spectra show no evidence for a thermal population of the high-spin state below 450 K.

At this stage, the extraordinary behaviour of the $[Fe(terpy)_2]^{2+}$ complex has to be attributed to a breakdown of the single mode model, that is, for $[Fe(terpy)_2]^{2+}$ there must be more than one normal mode with a significant contribution to the reaction coordinate. In order to check this hypothesis, DFT calculations using the RPBE functional, which gave good results for the $[Fe(bpy)_3]^{2+}$ complex, were also performed on $[Fe(terpy)_2]^{2+}$. Table 3 shows selected bond lengths and bond angles for the $[Fe(terpy)_2]^{2+}$ complex for the low-spin state and for the two components of the high-spin state in the D_{2d} point group. The relative electronic energies, ΔE^{el}_{HL}, of the two components of the high-spin state with respect to the low-spin state are also given. They remain relatively close to the RPBE ΔE^{el}_{HL} value found for $[Fe(bpy)_3]^{2+}$, which is to be expected for the two chemically very similar polypyridinyl complexes. With regard to the structural parameters, the optimised values obtained for the low-spin state agree well with the experimental values [30]. It should be noted that in the low-spin state, the tri-dentate terpyridine ligand is rather strained. Nevertheless, both bond lengths are in the range typical for

Table 3
Selected bond lengths (Å) and angles (°) for $[Fe(terpy)_2]^{2+}$: experimental data from Ref. [30], computational results using the RPBE functional and the TZP basis set as implemented in ADF

	Experimental	$^1A_1$	$^5B_2$	^5E
Fe–N, Fe–N″	1.988	2.009	2.217	2.223
Fe–N′	1.892	1.901	2.183	2.127
N–Fe–N′, N′–Fe–N″	80.6	80.6	73.4	74.6
N–C_2–C'_2–N′, N′–C'_6–C''_2–N″	1.8	0.0	0.0	0.0
∠(C_2–C'_2, C'_6–C''_2)		102.8	108.0	108.6
ΔE^{el}_{HL}			7631	8595

See Fig. 9 for the atom labelling. The values found for the electronic energy difference ΔE^{el}_{HL} (cm^{-1}) between the high-spin and low-spin states are also given.

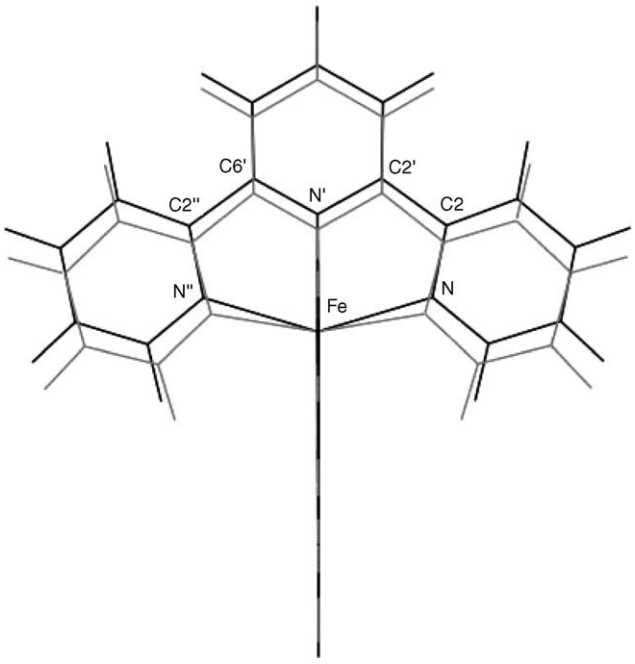

Fig. 9. Superposition of the geometry of the high-spin (black) and the low-spin (grey) states for $[Fe(terpy)_2]^{2+}$ calculated by DFT, projection perpendicular to the C_2 axis (RPBE/TZP).

low-spin complexes. As expected, the Fe–N bond lengths are considerably larger for the high-spin state. For the equatorial nitrogen atoms, the difference between the lower energy component of the high-spin state, the $^5B_2$ component, and the low-spin state is $\Delta r_{HL}^{eq} = 0.20$ Å, corresponding perfectly to the model value. For the axial nitrogen atoms this is no longer the case. The bond length difference $\Delta r_{HL}^{ax} = 0.28$ Å is much larger than the model value. Fig. 9 shows the superposition of the two structures. One immediately notes that not only the Fe–N bond lengths change on going from the low-spin to the high-spin state, but that in the high-spin state the tri-dentate ligand is much less strained. In fact, the reaction coordinate can qualitatively be broken down into the breathing mode plus bending modes involving the rings and exemplified by the angle between the inter-ring bonds (C_2–C_2') and (C_2''–C_6''). Thus, there are at least two normal modes with certainly quite different vibrational frequencies contributing to the reaction coordinate with substantial Huang–Rhys factors. This is schematically shown in Fig. 10. Provided the Huang–Rhys factor of the breathing mode does not significantly change from the model value of 45 as outlined in Section 2.1, the additional bending mode results in a substantial increase in the barrier height and therefore effectively slows down the relaxation process.

In the two mode model the low-temperature tunnelling rate constant is given by [31]

$$k_{HL}(T \to 0) = \frac{2\pi}{\hbar^2\omega_1}\beta_{HL}^2 \sum_{n_1,n_2} |\langle\chi_{n_1}|\chi_0\rangle|^2 |\langle\chi_{n_2}|\chi_0\rangle|^2 \delta(\Delta E_{HL}^0 - n_1\hbar\omega - n_2\hbar\omega_2) \quad (8)$$

where $\hbar\omega_1$ is the larger of the two frequencies and where the sum goes over all pairs of vibrational quanta n_1 and n_2 of the two modes satisfying energy conservation according to

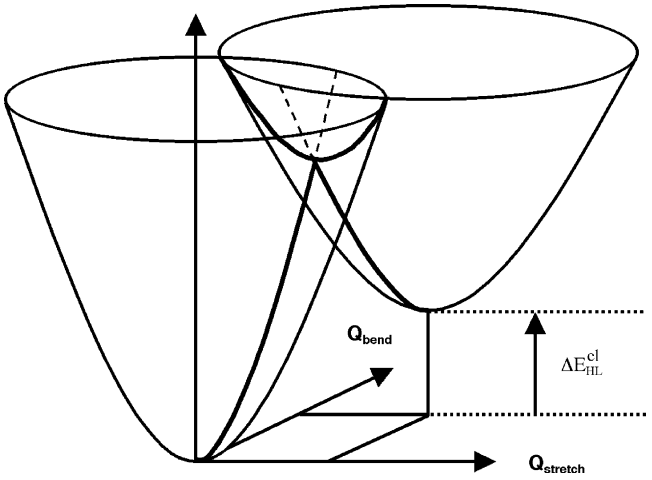

Fig. 10. Two mode model, the additional bending mode effectively increases the barrier height and thereby slows down the relaxation provided the Huang–Rhys factor for the breathing mode is not reduced.

$$\hbar\omega_1 n_1 + \hbar\omega_2 n_2 = \Delta E_{HL}^0 \quad (9)$$

In principle, Buhks et al. [9] have shown how to evaluate Eq. (8) even for an arbitrary number of normal modes contributing to the reaction coordinate using saddle point integration, and Vef et al. [32] have used it to describe the low-temperature tunnelling behaviour of the famous $[Fe(pic)_3]^{2+}$ (pic = 2-picolylamine) spin-crossover complex. A detailed normal mode decomposition of the reaction coordinate for the present system will be presented elsewhere [33]. Suffice to mention that the largest term in Eq. (8), given by the term with shortest pathway between the minima of the two potential wells, accounts for more than 50% of the sum

$$k_{HL}(T \to 0) \geq \frac{2\pi}{\hbar^2\omega_1} \frac{e^{-S_1} S_1^{n_1}}{n_1!} \frac{e^{-S_2} S_2^{n_2}}{n_2!} \quad (10)$$

where n_1 and n_2 not only obey Eq. (9), but depend upon the two Huang–Rhys factors according to the relation [34]

$$\frac{n_1\hbar\omega_1}{S_1} \approx \frac{n_2\hbar\omega_2}{S_2} \quad (11)$$

Thus, if for the breathing mode the model values of $S_1 \approx 45$ and $\hbar\omega_1 \approx 250\,cm^{-1}$ for the Huang–Rhys factor and the vibrational frequency, respectively, are conserved, a comparatively small contribution of the bending mode brings down the low-temperature tunnelling rate constant by several orders of magnitude.

The key question to ask at this point is, why is this bending mode operative in the doped crystalline host matrices, much less operative in the neat iron(II) compound, and not at all operative in the frozen solution. Well, the calculations are performed for complexes in the gas phase, but in condensed media they can only deform according to the predictions of the gas phase if the medium can accommodate the deformation. This is certainly the case for the crystalline hosts as all three metal ions, zinc, manganese and cadmium have much larger metal–nitrogen bond

lengths than iron(II) in the low-spin state. In fact, the zinc complex of a given ligand very often has the same metal–ligand bond length as the corresponding iron(II) complex in the high-spin state, and the corresponding manganese and cadmium complexes have still larger bond lengths. The lattice of the neat iron(II) complex is much more adapted to the low-spin state and the anisotropic expansion for the high-spin state is strongly hindered. Frozen solutions constitute a very rigid environment, and the anisotropic and large bond length change of the axial ligands when passing to the high-spin state is completely hindered.

3. Conclusions

In conclusion, the extrapolation of the energy gap rule, as worked out for spin-crossover complexes, to low-spin complexes works for isotropic systems, that is, for systems for which the reaction coordinate is well described by the totally symmetric breathing mode. If such is the case, kinetic data allows the determination of the energy of the spectroscopically dark high-spin state, which is not otherwise accessible.

For the $[Fe(bpy)_3]^{2+}$ complex, DFT calculations validate the structural hypothesis for $\Delta r_{HL} \approx 0.2$ Å. Furthermore, the geometry optimisation in the high-spin state indicated no spontaneous deviation from D_3, that is, the Jahn–Teller effect in the high-spin state is negligible. With regard to the zero-point energy difference between the two states, ΔE^0_{HL}, the performance of modern functionals puts the calculated values into the right ballpark. But calculated values are for the gas phase, experimental values are for the solid state, and solid state effects modulate ΔE^0_{HL} by several thousand wavenumbers. This constitutes an inherent difficulty with regard to the comparison of computational results with experimental data. In a next step it is imperative to perform calculations which take the environment into account correctly. This is computationally demanding and not straightforward.

For the tri-dentate ligand in the low-spin complex $[Fe(terpy)_2]^{2+}$ the extrapolation breaks down! DFT structure optimisation of the two states suggests that this is due to the anisotropic changes in the Fe–N bond lengths, with the change for the axial nitrogen atom of 0.28 Å exceeding the model value of 0.2 Å considerably. For such an anisotropic expansion of the coordination sphere the single mode model is clearly inadequate. The additional large difference in the axial Fe–N bond length results in a significant increase in the barrier between the two states, and thus slows down the relaxation at low temperatures by several orders of magnitude. From a practical point of view this opens a new avenue to search for complexes with a slow relaxation at higher temperatures than thought possible based on the single mode model.

Experimentally, transient EXAFS spectroscopy making use of synchrotron radiation, constitutes a new tool, which allows the determination of geometry differences of transient species in dilute systems such as the mixed crystalline solids or in amorphous media. Transient structural investigations will be important for the development of the research field not only to validate the DFT calculations presented here, but to actually probe the reaction coordinates in real time.

4. Experimental methods and computational details

4.1. Experimental methods

Most of the relaxation work was performed on dilute single crystals. In the absence of cooperative effects this results in gradual spin transitions with a well defined transition temperature, single exponential decay curves rather than the self-accelerated curves often observed for neat crystalline materials [11] and no interference from crystallographic phase transitions [35] nor deviations from single exponential decay due to inhomogeneous distributions in amorphous matrices [36].

Single crystals of $[M(bpy)_3](PF_6)_2$, M = Co, Zn, Mn, Cd, and $[M(terpy)_2](PF_6)_2$, M = Zn, Mn, Cd doped with ~0.05 mol% $[Fe(bpy)_3]^{2+}$ and $[Fe(terpy)_2]^{2+}$, respectively, were grown by isothermal diffusion of ether into acetonitrile/methanol solutions. Elemental analysis showed that there are no solvent molecules incorporated.

For the slow kinetics irradiation was effected using an Argon/Krypton mixed gas laser ($\lambda = 530$ nm, $I = 1$ mW/mm^2). The decay was followed by recording full spectra in given time intervals using a home-built set-up with a W-halogen lamp as light source, a single 0.28 m monochromator for light dispersion (Spex 280m) and a CCD (Jobin Yvon) for detection, all piloted by a Macintosh personal computer running a custom built program [37]. For fast decays the excitation was effected at 532 nm from the second harmonic of a pulsed Nd:YAG laser (Quantel Brillant) and the transmission was followed at a single wavelength with the same set-up as above but using a photomultiplier (Hamamatsu R928) with a fast preamplifier (LeCroy) and a digital oscilloscope (Tektronix TDK) instead of the CCD. Temperatures down to 11 K were effected with a closed cycle cryostat (Oxford Instruments CCC1202) with the sample sitting in Helium exchange gas for efficient cooling.

4.2. Computational details

For characterising $[Fe(bpy)_3]^{2+}$ in the low-spin and high-spin states [26], calculations were carried out using different functionals and basis sets of different types and qualities as implemented in the Amsterdam density functional (ADF) [24] and the Gaussian [23] program packages. The ADF package was used to perform calculations with the BP86, PBE, PW91 and RPBE GGA functionals. For all atoms, we used either the Slater-type orbital (STO) DZ basis set of valence double-ζ quality or the STO TZP basis set of valence triple-ζ polarised quality taken from the ADF basis set database. Gaussian was used to perform calculations with the B3LYP, B3LYP* and PBE0 hybrid functionals and the PBE GGA, using for all atoms the Gaussian-type orbital (GTO) TZVP basis set of valence triple-ζ polarised quality, or the 6-311+G** GTO basis set which is a triple-ζ polarised basis sets with sets of diffuse functions on the Fe, N and C atoms. The results reported here are those obtained with the TZP and TZVP basis sets which prove to be of very similar quality [26]. For the DFT study of $[Fe(terpy)_2]^{2+}$ in the two spin-states, the calculations were carried out with the ADF package using the RPBE functional and the TZP basis set. In all cases,

the symmetry of the $[Fe(bpy)_3]^{2+}$ and $[Fe(terpy)_2]^{2+}$ complexes were constrained to D_3 and D_{2d}, respectively. The calculations were run restricted for the low-spin state, and unrestricted for the high-spin state while constraining the projection of the total electronic spin along a reference axis to $M_S = 0$ and $M_S = +2$, respectively.

Acknowledgements

We thank the Swiss National Science Foundation for financial support, the "Centro Svizzero di Calcolo Scientifico" for computational resources, and G. La Macchia for assistance in the computations.

References

[1] P. Gütlich, H.A. Goodwin (Eds.), Spin Crossover in Transition Metal Complexes, vols. I–III, Springer, Heidelberg, 2004, Top. Curr. Chem., 233–235.
[2] (a) M.A. Hoselton, L.J. Wilson, R.S. Drago, J. Am. Chem. Soc. 97 (1975) 1722;
(b) B.A. Katz, C.E. Strouse, J. Am. Chem. Soc. 101 (1979) 6214;
(c) M. Mikami, Konno, Y. Saito, Acta Cryst. B 38 (1982) 452;
(d) E.A. Binstead, J.K. Beattie, Inorg. Chem. 25 (1986) 1481;
(e) J.F. Létard, P. Guionneau, L. Rabardel, J.A.K. Howard, A.E. Goeta, D. Chasseau, O. Kahn, Inorg. Chem. 37 (1998) 4432;
(f) P. van Koningsbruggen, Y. Garcia, O. Kahn, L. Fournes, H. Kooijman, A.L. Spek, J.G. Haasnoot, J. Moscovici, K. Provost, A. Michalowicz, F. Renz, P. Gütlich, Inorg. Chem. 39 (2000) 1891;
(g) D. Chernyshov, M. Hostettler, K.W. Törnroos, H.-B. Bürgi, Angew. Chem. 42 (2003) 3825.
[3] (a) J.K. McCusker, K.N. Walda, R.C. Dunn, J.D. Simon, D. Magde, D.N. Hendrickson, J. Am. Chem. Soc. 114 (1992) 6919;
(b) J.K. McCusker, J.N. Walda, R.C. Dunn, J.D. Simon, D. Magde, D.N. Hendrickson, J. Am. Chem. Soc. 115 (1993) 298.
[4] (a) C. Brady, H. Toftlund, J.J. McGarvey, J.K. McCusker, D.N. Hendrickson, in: P. Gütlich, H.A. Goodwin (Eds.), Spin-crossover in Transition Metal Compounds, vol. III, Springer, Berlin, 2004, p. 1, Top. Curr. Chem., 235, and references therein;
(b) I. Lawthers, J.J. McGarvey, J. Am. Chem. Soc. 106 (1984) 4280;
(c) J.J. McGarvey, I. Lawthers, J. Chem. Soc., Chem. Commun. (1982) 906.
[5] J.K. Beattie, Adv. Inorg. Chem. 32 (1988) 1.
[6] (a) S. Decurtins, P. Gütlich, C.P. Köhler, H. Spiering, A. Hauser, Chem. Phys. Lett. 13 (1984) 1;
(b) S. Decurtins, P. Gütlich, K.M. Hasselbach, H. Spiering, A. Hauser, Inorg. Chem. 24 (1985) 2174;
(c) A. Hauser, Chem. Phys. Lett. 124 (1986) 543.
[7] (a) S. Decurtins, P. Gütlich, C.P. Koehler, H. Spiering, J. Chem. Soc., Chem. Commun. (1985) 430;
(b) N. Moliner, A.B. Gaspar, M.C. Munoz, V. Niel, J. Cano, J.A. Real, Inorg. Chem. 40 (2001) 3986;
(c) L. Capes, J.F. Létard, O. Kahn, Chem. Eur. J. 6 (2000) 2246;
(d) S. Hayami, Z. Gu, Y. Einaga, Y. Kobayashi, Y. Ishikawa, Y. Yamada, A. Fujishima, O. Sato, Inorg. Chem. 40 (2001) 3240;
(e) R.H. Herber, Inorg. Chem. 26 (1987) 173;
(f) D.C. Figg, R.H. Herber, J.A. Potenza, Inorg. Chem. 31 (1992) 2111;
(g) N. Moliner, L. Salmon, L. Capes, M.C. Munoz, J.F. Létard, A. Bousseksou, J.P. Tuchagues, J.J. McGarvey, A.C. Dennis, M. Castro, R. Burriel, J.A. Real, J. Phys. Chem. B 106 (2002) 4276, and many more!.
[8] (a) J. Kusz, H. Spiering, P. Gütlich, J. Appl. Cryst. 33 (2000) 201;
(b) J. Kusz, H. Spiering, P. Gütlich, J. Appl. Cryst. 34 (2001) 229;
(c) V. Niel, A.L. Thompson, A.E. Goeta, C. Enachescu, A. Hauser, A. Galet, M.C. Muñoz, J.A. Real, Chem. Eur. J. 11 (2005) 2047;
(d) J. Kusz, D. Schollmeyer, H. Spiering, P. Gütlich, J. Appl. Cryst. 38 (2005) 528.
[9] E. Buhks, G. Navon, M. Bixon, J. Jortner, J. Am. Chem. Soc. 102 (1980) 2918.
[10] C.-L. Xie, D.N. Hendrickson, J. Am. Chem. Soc. 109 (1987) 6981.
[11] A. Hauser, in: P. Gütlich, H.A. Goodwin (Eds.), Spin-crossover in Transition Metal Compounds, vol. II, Springer, Berlin, 2004, p. 155, Top. Curr. Chem., 234, and references therein.
[12] (a) L. Wiehl, H. Spiering, P. Gütlich, K. Knorr, J. Appl. Cryst. 23 (1990) 151;
(b) L. Wiehl, G. Kiel, C.P. Köhler, H. Spiering, P. Gütlich, Inorg. Chem. 25 (1986) 1565;
(c) L. Wiehl, Acta Cryst. B 49 (1993) 289.
[13] C.J. Donnelly, G.F. Imbusch, in: B. DiBartolo (Ed.), NATO ASI B 245, Plenum Press, New York, 1991, p. 175.
[14] (a) T.C. Brunold, H.U. Güdel, in: E.I. Solomon, A.B.P. Lever (Eds.), Inorganic Electronic Structure and Spectroscopy, vol. I, Wiley, New York, 1999, p. 259;
(b) C.W. Struck, W.H. Fonger, Understanding Luminescence Spectra and Efficiencies Using Wp and Related Functions, Springer, Heidelberg, 1991.
[15] (a) P. Suppan, Topics in Current Chemistry 163, Springer, Heidelberg, 1992, p. 95;
(b) P. Barbara, T.J. Meyer, M.A. Ratner, J. Phys. Chem. 100 (1996) 13148.
[16] A. Hauser, N. Amstutz, S. Delahaye, S. Schenker, A. Sadki, R. Sieber, M. Zerara, in: Th. Schönherr (Ed.), Structure and Bonding, 106, Springer, Berlin, 2004, p. 81.
[17] A.D. Kirk, P.E. Hoggard, G.B. Porter, M.G. Rockley, M.W. Windsor, Chem. Phys. Lett. 37 (1976) 199.
[18] S. Deisenroth, A. Hauser, H. Spiering, P. Gütlich, Hyperf. Interact. 93 (1994) 1573.
[19] P. Hohenberg, W. Kohn, Phys. Rev. 136 (1964) B864.
[20] W. Kohn, L.J. Sham, Phys. Rev. 140 (1965) A1133.
[21] O. Gunnarsson, B.I. Lundqvist, Phys. Rev. B 13 (1976) 4274.
[22] W. Koch, M.C. Holthausen, A Chemist's Guide to Density Functional Theory, Wiley/VCH, New York, 2000.
[23] M.J. Frisch, G.W. Trucks, H.B. Schlegel, G.E. Scuseria, M.A. Robb, J.R. Cheeseman, J.A. Montgomery Jr., T. Vreven, K.N. Kudin, J.C. Burant, J.M. Millam, S.S. Iyengar, J. Tomasi, V. Barone, B. Mennucci, M. Cossi, G. Scalmani, N. Rega, G.A. Petersson, H. Nakatsuji, M. Hada, M. Ehara, K. Toyota, R. Fukuda, J. Hasegawa, M. Ishida, T. Nakajima, Y. Honda, O. Kitao, H. Nakai, M. Klene, X. Li, J.E. Knox, H.P. Hratchian, J.B. Cross, V. Bakken, C. Adamo, J. Jaramillo, R. Gomperts, R.E. Stratmann, O. Yazyev, A.J. Austin, R. Cammi, C. Pomelli, J.W. Ochterski, P.Y. Ayala, K. Morokuma, G.A. Voth, P. Salvador, J.J. Dannenberg, V.G. Zakrzewski, S. Dapprich, A.D. Daniels, M.C. Strain, O. Farkas, D.K. Malick, A.D. Rabuck, K. Raghavachari, J.B. Foresman, J.V. Ortiz, Q. Cui, A.G. Baboul, S. Clifford, J. Cioslowski, B.B. Stefanov, G. Liu, A. Liashenko, P. Piskorz, I. Komaromi, R.L. Martin, D.J. Fox, T. Keith, M.A. Al-Laham, C.Y. Peng, A. Nanayakkara, M. Challacombe, P.M.W. Gill, B. Johnson, W. Chen, M.W. Wong, C. Gonzalez, J.A. Pople, Gaussian 03 (Revision B.03/B.04), Gaussian, Inc., Wallingford, CT, 2004.
[24] Amsterdam Density Functional Program, Release ADF2004.01, Theoretical Chemistry, Vrije Universiteit, Amsterdam, The Netherlands. http://www.scm.com.
[25] G. te Velde, F.M. Bickelhaupt, E.J. Baerends, C. Fonseca Guerra, S.J.A. van Gisbergen, J.G. Snijders, T. Ziegler, J. Comp. Chem. 22 (2001) 931.
[26] M.L. Lawson Daku, A. Vargas, A. Hauser, A. Fouqueau, M.E. Casida, Chem. Phys. Chem. 6 (2005) 1393.
[27] S. Dick, Z. Kristallogr.: New Cryst. Struct. 213 (1998) 356.
[28] (a) A. Fouqueau, S. Mer, M.E. Casida, L.M. Lawson Daku, A. Hauser, T. Minerva, F. Neese, J. Chem. Phys. 120 (2004) 9473;
(b) A. Fouqueau, M.E. Casida, L.M. Lawson Daku, A. Hauser, F. Neese, J. Chem. Phys. 122 (2005) 044110.
[29] (a) F. Renz, H. Oshio, H. Spiering, V. Ksenofotnov, M. Waldeck, H. Spiering, P. Gütlich, Angew. Chem. Int. Ed. 39 (2000) 3699;

(b) H. Oshio, H. Spiering, V. Ksenofotnov, F. Renz, P. Gütlich, Inorg. Chem. 40 (2001) 1143.
[30] A.T. Baker, H.A. Goodwin, Aust. J. Chem. 38 (1985) 207.
[31] P. Avouris, W.M. Gelbart, M.A. El-Sayed, Chem. Rev. 77 (1977) 793.
[32] A. Vef, U. Manthe, P. Gütlich, A. Hauser, J. Chem. Phys. 101 (1994) 9326.
[33] M. Lawson, A. Hauser, in preparation.
[34] Empirical relation derived numerically, approximately valid for large values of *S*.
[35] J. Jeftic, A. Hauser, J. Phys. Chem. B 101 (1997) 10262.
[36] A. Hauser, J. Adler, P. Gütlich, Chem. Phys. Lett. 152 (1988) 468.
[37] U. Oetliker, program platform for optical spectroscopy, Geneva 1998.